Probing spectral properties of radio-quiet quasars searched for optical microvariability – II

Ravi Joshi,[1][*] Hum Chand,[1][*] Paul J. Wiita,[2][*] Alok C. Gupta[1][*]
and Raghunathan Srianand[3][*]

[1]*Aryabhatta Research Institute of Observational Sciences (ARIES), Manora Peak, Nainital 263129, India*
[2]*Department of Physics, The College of New Jersey, PO Box 7718, Ewing, NJ 08628-0718, USA*
[3]*IUCAA, Postbag 4, Ganeshkhind, Pune 411 007, India*

ABSTRACT

In the context of active galactic nucleus (AGN) unification schemes, rapid variability properties play an important role in understanding any intrinsic differences between sources in different classes. In this respect, any clue based on spectral properties will be very useful toward understanding the mechanisms responsible for the origin of rapid small-scale optical variations or microvariability. Here we have added spectra of 46 radio-quiet quasars (RQQSOs) and Seyfert 1 galaxies to those of our previous sample of 37 such objects, all of which had been previously searched for microvariability. We took new optical spectra of 33 objects and obtained 13 others from the literature. Their $H\beta$ and Mg II emission lines were carefully fitted to determine line widths (FWHM) as well as equivalent widths (EW) due to the broad emission-line components. The line widths were used to estimate black hole masses and Eddington ratios, ℓ. Both EW and FWHM are anticorrelated with ℓ. Nearly all trends were in agreement with our previous work, although the tendency for sources exhibiting microvariability to be of lower luminosity was not confirmed. Most importantly, this whole sample of EW distributions provides no evidence for the hypothesis that a weak jet component in radio-quiet AGNs is responsible for their microvariability.

Key words: galaxies: active – quasars: emission lines – quasars: general.

1 INTRODUCTION

Rapid small-scale optical variations or intranight microvariability are well-known characteristics of active galactic nuclei (AGNs), but the processes causing the bulk of these microvariations are still a matter of debate. The variability mechanisms in radio-loud objects are widely believed to be connected to conditions in relativistic jets. However, it is still unclear whether in radio-quiet objects the nature of intranight variability is different, or whether a faint, variable jet is also a dominant component for these objects. Czerny et al. (2008) tried to understand the microvariation mechanism within the framework of the following scenarios: (i) fluctuations from an accretion disc (Mangalam & Wiita 1993), (ii) irradiation of an accretion disc by a variable X-ray flux (Rokaki, Collin-Souffrin & Magnan 1993; Gaskell 2006) and (iii) the presence of modestly misaligned jets in radio-quiet quasars or a 'blazar component' (Gopal-Krishna et al. 2003). They concluded that the blazar-component model is the most promising to give rise to intranight optical variability (INOV).

In this blazar-component scenario, the spectral properties of sources can play a crucial role in constraining the models further. For instance, if blazar components dominate the variability of RQQSOs then, due to the increase in the continuum produced by the jets, one expects smaller equivalent widths (EW) of prominent emission lines such as $H\beta$ and Mg II for sources with microvaraibility compared with their average value in a sample including non-variable sources. Recently, in Chand, Wiita & Gupta (2010; hereafter Paper I), we have worked toward this goal by exploiting the optical spectra available from the Sloan Digital Sky Survey, Data Release 7 (SDSS DR-7: Abazajian et al. 2009). We carried out careful spectral modelling of the $H\beta$ and Mg II emission-line regions for RQQSO and Seyfert 1 samples already searched for microvariability (hereafter referred to collectively as RQQSOs). In Paper I, we first investigated any effect of key spectral parameters (e.g. EW and FWHM) on the microvariability of RQQSOs. Secondly, we estimated other relevant AGN parameters such as the black hole mass $M_{\rm bh}$ and Eddington ratios. To do this, their $H\beta$ and Mg II emission lines were carefully fitted to determine line widths (FWHM) as well as equivalent widths (EW) due to the broad emission-line components. The line widths were used to estimate black hole masses and Eddington ratios. The EW distributions did not provide evidence for the hypothesis that a

[*]E-mail: ravi@aries.res.in (RJ); hum@aries.res.in (HC); wiitap@tcnj.edu (PJW); alok@aries.res.in (ACG); anand@iucaa.ernet.in (RS)

weak jet component in RQQSOs is responsible for their microvari-ability, and perhaps instead it may indicate that variations involving the accretion disc (e.g. Wiita 2006) are important for them. We also concluded that there may be a weak negative correlation between Hβ EW and ℓ, but there is a significant one between the Mg II EW and ℓ. In addition, we noted that there is a tendency for sources with detectable optical microvariability to have somewhat lower luminosities than those with no such detections (see fig. 8 of Paper I).

All the above tentative conclusions from our Paper I were certainly interesting; however, as we stressed there, it is very important that they should be tested by examining larger samples. The importance of a larger sample for such investigations is evident from our recent finding on the fraction of broad absorption-line QSOs showing microvariability (Joshi et al. 2011). That fraction appeared to be 50 per cent based on only six sources but, using a larger sample of 23 sources, Joshi et al. (2011) found it to be around 10 per cent, similar to RQQSOs (Gupta & Joshi 2005).

Therefore, given the important implications of our above results, based on spectral analysis of 37 sources, for the origin of RQQSO microvariability and hence processes in the accretion disc itself, it becomes important to carry out spectral analyses of as many sources searched for microvariability as possible. The obvious source for such a sample would be the remainder of the objects from the total of 117 sources in the compilation of Carini et al. (2007) for which SDSS DR-7 spectra are not available. This forms the main motivation of this paper, in which we more than double the sample size by taking new spectra and gathering others from the literature that we then analyse. Results from this larger sample can test the validity of results found using our previous modest sample in Paper I.

This paper is organized as follows. Section 2 describes the data sample and selection criteria. Section 3 describes the observations and data reduction while Section 4 gives details of our spectral fitting procedure. In Section 5 we focus on black hole (BH) mass measurements and in Section 6 we give estimates of Eddington ratios and BH growth times. Section 7 gives a discussion and conclusions. Throughout, we have used flat cosmology with $H_0 = 70 \, \mathrm{km \, s^{-1} \, Mpc^{-1}}$, $\Omega_m = 0.3$ and $\Omega_\Lambda = 0.7$.

2 DATA SAMPLE AND SELECTION CRITERIA

From the compilation of 117 radio-quiet AGNs in Carini et al. (2007), which were often extensively searched for microvariability, Paper I analysed 33 sources (from a total sample of 37 sources) for which SDSS DR7 spectra were available. Here we examined the rest of the the 84 sources and, using their redshifts, found that among them 25 sources are such that neither their Hβ nor Mg II lines fall in the optical spectral range, as they have redshifts outside the following respective ranges: $z \leq 0.65; 0.43 \leq z \leq 1.86$. For the remaining 59 sources we found that Hβ and Mg II emission lines fall in the spectral range of 3800–8300 Å for 50 and 9 sources, respectively.

We have searched for the optical spectra of these 59 sources in SDSS DR8 (Aihara et al. 2011) as well as in the NASA/IPAC Extragalactic Database (NED). We could find SDSS DR8 spectra for eight sources and NED spectra with the desired quality (good signal-to-noise ratio and spectral coverage for the Mg II or Hβ line) for five sources, as listed in Table 1.

We planned the observations of the remainder of the 46 sources, using the IUCAA Faint Object Spectrograph (IFOSC) mounted on the 2-m telescope at IUCAA Girawali Observatory (IGO), near Pune, India. With IGO we could obtain the desired spectra for 33 sources. Among the remaining 13 sources, six were not visible from IGO, having very negative declinations, four (J001555.1+023024, J012017.2+213346, J220311.5−180143 and J194240.6−101925) could not be observed due to either non-visibility or lack of enough observing time, one, namely J103206.2+324015, was classified as a white dwarf in NED and the remaining two, J082740.2+094208 and J154559.1+270630, though observed, were dropped from our analysis as they showed very poor Hβ lines in their spectra.

Finally, we are left with a sample of 46 sources (33 new observations, eight from SDSS DR8 and five from NED); among them, 42 spectra cover Hβ lines while 4 spectra cover Mg II doublet lines. The source information is listed in Table 1. The first four columns give source name, RA (J2000), Dec. (J2000) and emission redshift (z_{em}), while the fifth column provides the apparent magnitude in either B or V band. The sixth column provides the absolute B magnitudes and the seventh column indicates microvariability detection status; the eighth column gives a source classification from among classes such as QSO, broad absorption-line QSO (BALQSO) or Seyfert (Sy) galaxy type. In the last column we have given the spectral resource information.

3 OBSERVATIONS AND DATA REDUCTION

The new spectra were obtained for 33 sources. The observations were carried out using the IFOSC mounted on the 2-m IGO telescope. We took long-slit spectra covering the wavelength range 3800–6840 Å using the GR7 grism and 5800–8300 Å using the GR8 grism of the IFOSC to cover the Mg II and Hβ lines, respectively, as noted in the third column of the observing log in Table 2. A slit width of either 1.0 or 1.5 arcsec was used, as listed in the fourth column of Table 2. Typical seeing during our observations was around 1.2–1.3 arcsec. The raw CCD frames were cleaned using standard IRAF[1] procedures. We used halogen flats for flat-fielding the frames. Since at $\lambda > 7000$ Å simple flat-fielding does not remove the fringes, in the case of grism GR8 the QSO was moved along the slit for two different exposures at the same position angle. We subsequently removed fringing by subtracting one frame from the other taken on the same night. The same procedure was applied to standard stars as well. We then extracted the one-dimensional spectrum from individual frames using the IRAF task 'doslit'. Wavelength calibration of the spectra was performed using helium–neon lamps. The spectrophotometric flux calibration was done using standard stars and assuming a mean extinction for the IGO site. In cases when multiple exposures were needed, we coadded the flux with $1/\sigma_i^2$ weightage, where σ_i is the error in an individual pixel. The error spectrum was computed taking into account proper error propagation during the combining process. The typical median signal-to-noise ratio (SNR) over the spectral fitting range of our sample varies from 20–150 per pixel, as listed in the last column of Table 2. Our spectral range also covers atmospheric absorption-line regions but in all cases our fitting regions fall either blueward or redward of them, so we need not correct for any blending due to them in our analyses.

---

[1] IRAF is distributed by the National Optical Astronomy Observatories, which are operated by the Association of Universities for Research in Astronomy, Inc., under cooperative agreement with the National Science Foundation.

Table 1. New sample of radio-quiet QSOs and Seyfert galaxies from the compilation of Carini et al. (2007).

QSO Name[a] (1)	α_{2000} (2)	δ_{2000} (3)	z_{em}[b] (4)	$m^\star_{(band)}$ (5)	$M^\star_B$ (6)	Variable? (7)	Class (8)	Spectra[c] (9)
J000619.5+201210	$00^h\ 06^m\ 19.5^s$	$+20°\ 12'\ 10''$	0.025	$13.75_{(B)}$	−22.14	N	SY1.2	IGO
J002913.6+131603	$00^h\ 29^m\ 13.6^s$	$+13°\ 16'\ 03''$	0.142	$16.30_{(V)}$	−24.70	Y	SY1	IGO
J004547.3+041024	$00^h\ 45^m\ 47.3^s$	$+04°\ 10'\ 24''$	0.385	$15.88_{(B)}$	−26.00	N	BALQSO	IGO
J005334.9+124136	$00^h\ 53^m\ 34.9^s$	$+12°\ 41'\ 36''$	0.058	$14.39_{(B)}$	−24.43	N	SY1	IGO
J005452.1+252538	$00^h\ 54^m\ 52.1^s$	$+25°\ 25'\ 38''$	0.154	$15.42_{(B)}$	−24.40	N	SY1	IGO
J011354.5+390744	$01^h\ 13^m\ 54.5^s$	$+39°\ 07'\ 44''$	0.234	$16.70_{(B)}$	−24.10	N	SY1	IGO
J012240.6+231015	$01^h\ 22^m\ 40.6^s$	$+23°\ 10'\ 15''$	0.052	$15.41_{(B)}$	−22.12	N	SY1	IGO
J051611.4−000859	$05^h\ 16^m\ 11.4^s$	$-00°\ 08'\ 59''$	0.032	$14.10_{(B)}$	−25.20	Y	SY1	IGO
J051633.4−002713	$05^h\ 16^m\ 33.4^s$	$-00°\ 27'\ 13''$	0.292	$16.26_{(B)}$	−25.10	N	SY1.2	IGO
J055453.6+462622	$05^h\ 54^m\ 53.6^s$	$+46°\ 26'\ 22''$	0.020	$15.00_{(B)}$	−22.60	N	SY1	IGO
J071415.1+454156	$07^h\ 14^m\ 15.1^s$	$+45°\ 41'\ 56''$	0.055	$14.90_{(B)}$	−29.60	N	SY1.5	IGO
J073657.0+584613	$07^h\ 36^m\ 57.0^s$	$+58°\ 46'\ 13''$	0.039	$15.29_{(B)}$	−21.80	N	SY1.5	IGO
J084742.4+344504	$08^h\ 47^m\ 42.4^s$	$+34°\ 45'\ 04''$	0.064	$14.00_{(B)}$	−23.95	Y	SY1	IGO
J092512.9+521711	$09^h\ 25^m\ 12.9^s$	$+52°\ 17'\ 11''$	0.035	$15.62_{(B)}$	−21.00	Y	SY1	SDSS
J092603.3+124404	$09^h\ 26^m\ 03.3^s$	$+12°\ 44'\ 04''$	0.029	$14.93_{(B)}$	−21.27	N	SY1.2	SDSS
J095652.4+411522	$09^h\ 56^m\ 52.4^s$	$+41°\ 15'\ 22''$	0.234	$15.05_{(B)}$	−25.73	N	SY1	IGO
J101420.7−041840	$10^h\ 14^m\ 20.7^s$	$-04°\ 18'\ 40''$	0.058	$15.49_{(B)}$	−22.22	N	SY1	IGO
J105143.9+335927	$10^h\ 51^m\ 43.9^s$	$+33°\ 59'\ 27''$	0.167	$15.81_{(B)}$	−24.19	N	SY1	SDSS
J110631.8−005252	$11^h\ 06^m\ 31.8^s$	$-00°\ 52'\ 52''$	0.423	$16.02_{(B)}$	−25.70	Y	QSO	IGO
J111908.7+211918	$11^h\ 19^m\ 08.7^s$	$+21°\ 19'\ 18''$	0.176	$15.17_{(B)}$	−24.96	Y	SY1	IGO
J112147.1+114418	$11^h\ 21^m\ 47.1^s$	$+11°\ 44'\ 18''$	0.050	$14.65_{(B)}$	−22.69	N	SY1.2	IGO
J112302.3−273004	$11^h\ 23^m\ 02.3^s$	$-27°\ 30'\ 04''$	0.389	$16.80_{(V)}$	−25.20	N	QSO	IGO
J112439.2+420145	$11^h\ 24^m\ 39.2^s$	$+42°\ 01'\ 45''$	0.225	$16.02_{(B)}$	−24.71	N	SY 1	SDSS
J112731.9−304446	$11^h\ 27^m\ 31.9^s$	$-30°\ 44'\ 46''$	0.673	$16.30_{(V)}$	−27.00	N	QSO	IGO
J115349.3+112830	$11^h\ 53^m\ 49.3^s$	$+11°\ 28'\ 30''$	0.176	$15.51_{(B)}$	−24.61	N	SY 1	SDSS
J120309.6+443153	$12^h\ 03^m\ 09.6^s$	$+44°\ 31'\ 53''$	0.002	$13.74_{(B)}$	−17.40	N	SY1.5	NED[1]
J121032.6+392421	$12^h\ 10^m\ 32.6^s$	$+39°\ 24'\ 21''$	0.003	$11.50_{(B)}$	−20.60	N	SY1.5	IGO
J125048.3+395139	$12^h\ 50^m\ 48.3^s$	$+39°\ 51'\ 39''$	1.032	$16.06_{(V)}$	−27.86	N	QSO	SDSS
J125948.8+342323	$12^h\ 59^m\ 48.8^s$	$+34°\ 23'\ 23''$	1.375	$16.79_{(B)}$	−28.00	N	QSO	SDSS
J132349.5+654148	$13^h\ 23^m\ 49.5^s$	$+65°\ 41'\ 48''$	0.168	$15.86_{(B)}$	−24.23	N	SY1	IGO
J135458.7+005211	$13^h\ 54^m\ 58.7^s$	$+00°\ 52'\ 11''$	1.127	$16.00_{(V)}$	−28.06	N	QSO	IGO
J140516.2+255534	$14^h\ 05^m\ 16.2^s$	$+25°\ 55'\ 34''$	0.164	$15.57_{(B)}$	−24.46	N	SY1	IGO
J141348.3+440014	$14^h\ 13^m\ 48.3^s$	$+44°\ 00'\ 14''$	0.089	$14.99_{(B)}$	−23.68	N	SY1	IGO
J141700.7+445606	$14^h\ 17^m\ 00.7^s$	$+44°\ 56'\ 06''$	0.113	$15.74_{(B)}$	...	N	SY1	SDSS
J142906.6+011706	$14^h\ 29^m\ 06.6^s$	$+01°\ 17'\ 06''$	0.086	$15.05_{(B)}$	−23.51	N	SY1	IGO
J144207.4+352623	$14^h\ 42^m\ 07.4^s$	$+35°\ 26'\ 23''$	0.079	$15.00_{(B)}$	−23.32	N	SY1	IGO
J153638.3+543333	$15^h\ 36^m\ 38.3^s$	$+54°\ 33'\ 33''$	0.038	$15.31_{(B)}$	−21.48	N	SY1	IGO
J155202.3+201402	$15^h\ 52^m\ 02.3^s$	$+20°\ 14'\ 02''$	0.251	$17.40_{(V)}$	−24.60	N	QSO	IGO
J162011.3+172428	$16^h\ 20^m\ 11.3^s$	$+17°\ 24'\ 28''$	0.112	$15.53_{(B)}$	...	N	SY1	IGO
J170124.8+514920	$17^h\ 01^m\ 24.8^s$	$+51°\ 49'\ 20''$	0.292	$15.43_{(B)}$	−25.78	Y	BALQSO	NED[2]
J175116.6+504539	$17^h\ 51^m\ 16.6^s$	$+50°\ 45'\ 39''$	0.299	$15.80_{(B)}$	−25.60	Y	QSO	IGO
J211452.6+060742	$21^h\ 14^m\ 52.6^s$	$+06°\ 07'\ 42''$	0.466	$15.52_{(B)}$	−26.70	N	QSO	IGO
J213227.8+100819	$21^h\ 32^m\ 27.8^s$	$+10°\ 08'\ 19''$	0.062	$14.62_{(B)}$	−23.20	N	QSO	NED[3]
J221712.2+141421	$22^h\ 17^m\ 12.2^s$	$+14°\ 14'\ 21''$	0.065	$14.98_{(B)}$	−23.04	N	QSO	NED[4]
J230315.6+085226	$23^h\ 03^m\ 15.6^s$	$+08°\ 52'\ 26''$	0.016	$13.00_{(B)}$	−22.10	Y	SY1.2	NED[5]
J230702.9+043257	$23^h\ 07^m\ 02.9^s$	$+04°\ 32'\ 57''$	0.046	$15.44_{(B)}$	−21.57	N	SY1	IGO

[a]Object name in J2000.

[b]Redshift as determined from the peak of the O IIIλ5007 emission line.

[*]Apparent magnitudes (m_B or m_V) and absolute magnitudes (M_B) are taken from Carini et al. (2007).

[c]NED spectral references: [1]Moustakas & Kennicutt (2006); [2,3,4]Boroson & Green (1992); [5]Kim et al. (1995).

4 LINE ANALYSIS THROUGH SIMULTANEOUS SPECTRAL FITTING

The Hβ and Mg II emission lines were carefully modelled using the fitting procedure described in Paper I. The spectra were first corrected for Galactic extinction using the extinction map of Schlegel, Finkbeiner & Davis (1998) and the reddening curve of Fitzpatrick (1999). Then they were transformed into the rest frame using the redshift as determined from the peak of the O III5007 emission line. Limited by the complications needed to fit the continuum and the Fe II emission, namely that (i) there are essentially no emission-

line-free regions where the continuum can be determined (Vanden Berk et al. 2001), (ii) Fe II features and their blending with Hβ and Mg II lines are prominent and (iii) the Hβ line is highly blended with O III$\lambda\lambda$4959,5007 lines, we have opted to carry out simultaneous fits[2] of continuum, Fe II emission, Hβ and Mg II and all other

---

[2] To carry out the simultaneous fit we have used the MPFIT package for nonlinear fitting, written in INTERACTIVE DATA LANGUAGE routines. MPFIT is kindly provided by Craig B. Markwardt and is available at http://cow.physics.wisc.edu/craigm/idl/.

Table 2. IGO observation log.

QSO Name	Date of Obs.	Grism	Slit width	SNR
J000619.5+201210	2009-12-13	IFOSC7	1.5″	82
J002913.6+131603	2009-12-13	IFOSC7	1.0″	73
J004547.3+041024	2009-12-12	IFOSC8	1.5″	38
J005334.9+124136	2009-12-13	IFOSC7	1.0″	80
J005452.1+252538	2009-12-12	IFOSC7	1.5″	40
J011354.5+390744	2011-01-06	IFOSC7	1.5″	19
J012240.6+231015	2011-02-05	IFOSC7	1.5″	47
J051611.4−000859	2011-01-06	IFOSC7	1.5″	127
J051633.4−002713	2009-12-12	IFOSC8	1.5″	43
J055453.6+462622	2009-12-13	IFOSC7	1.0″	47
J071415.1+454156	2011-02-04	IFOSC7	1.0″	54
J073657.0+584613	2011-02-05	IFOSC7	1.0″	63
J084742.4+344504	2009-12-12	IFOSC7	1.5″	92
J095652.4+411522	2009-12-13	IFOSC7	1.0″	44
J101420.7−041840	2011-02-05	IFOSC7	1.0″	67
J110631.8−005252	2011-04-01	IFOSC8	1.5″	39
J111908.7+211918	2010-04-18	IFOSC7	1.0″	32
J112147.1+114418	2011-02-04	IFOSC7	1.0″	41
J112302.3−273004	2011-04-01	IFOSC8	1.5″	73
J112731.9−304446	2010-04-19	IFOSC7	1.0″	42
J121032.6+392421	2010-04-18	IFOSC7	1.0″	21
J132349.5+654148	2011-02-04	IFOSC7	1.0″	150
J135458.7+005211	2011-03-30	IFOSC7	1.5″	37
J140516.2+255534	2011-02-04	IFOSC7	1.0″	51
J141348.3+440014	2010-04-17	IFOSC7	1.0″	40
J142906.6+011706	2010-04-18	IFOSC7	1.0″	31
J144207.4+352623	2010-04-17	IFOSC7	1.0″	50
J153638.3+543333	2010-04-17	IFOSC7	1.0″	37
J155202.3+201402	2011-02-05	IFOSC7	1.0″	23
J162011.3+172428	2010-04-18	IFOSC7	1.0″	23
J175116.6+504539	2011-03-30	IFOSC7	1.5″	55
J211452.6+060742	2009-12-12	IFOSC8	1.5″	38
J230702.9+043257	2009-12-14	IFOSC7	1.0″	20

metal emission lines present in the spectra. For this purpose we adopted the procedure described in detail in Paper I, which in brief is as follows.

4.1 Hβ region fit

(i) We fit the spectrum comprising the Hβ line in the rest wavelength range between 4435 and 5535 Å. The continuum in this region is modelled by a single power law, i.e. $a_1\lambda^{-\alpha}$.

(ii) The complex profile of the Hβ line is fitted with multiple (1–4) Gaussians with an initial guess of two narrow, one broad and one very broad component. To reduce the arbitrariness of the component fits and also to make the decomposition more physical, we have constrained the redshift and width of the two narrow components of Hβ to be the same as those of the O III$\lambda\lambda$4959,5007 lines. The line profiles of O IIIλ5007 and hence O IIIλ4959 are modelled as double Gaussians, with one stronger narrow component with width less than 2000 km s^{-1} and one weaker broader component with width less than 4000 km s^{-1}. However, if for some source spectra the second component is not statistically required, the procedure we use automatically drops it during the fit. So, we have only four free parameters, two for redshift and two for width of the O III$\lambda\lambda$4959,5007 and narrow Hβ components.

(iii) The optical Fe II emission is modelled as $C(\lambda) = c_b C_b(\lambda) + c_n C_n(\lambda)$, where $C_b(\lambda)$ represents the broad Fe II lines and $C_n(\lambda)$ the narrow Fe II lines, with the relative intensities fixed at those of I ZW 1, as given in tables A.1 and A.2 of Véron-Cetty, Joly & Véron

(2004). The redshifts of the broad Fe II lines and Hβ component are fitted as free parameters, while their widths are kept the same, with a constraint that they should be larger than 1000 km s^{-1}; this width is then used for estimating the BH masses. Similarly, for the narrow Fe II line the redshift is fitted as a free parameter but the width is kept the same as that of the stronger narrow O IIIλ5007 component. The fourth (very broad) Hβ component, if required for the fit, is subject only to the constraint that its width should be more than 1000 km s^{-1}. The emission lines other than Fe II and O III$\lambda\lambda$4959,5007 (see table 2 in Vanden Berk et al. 2001), are modelled with single Gaussians.

The final fit is achieved by simultaneously varying all the free parameters to minimize the χ^2 value until the reduced χ_r^2 is ≈ 1. Samples of our spectral fitting in the optical region are given for Hβ in Figs 1 and 2. The values for FWHM and EW (both the broad component EW$_B$ and the total EW$_{all}$) for the Hβ lines are given in Table 3.

4.2 Mg II doublet region fit

(i) We fit the spectrum comprising the Mg II doublet region in the rest wavelength range between 2200 and 3200 Å. The continuum in this region is modelled by a single power law, i.e. $a_1\lambda^{-\alpha}$.

(ii) For fitting the Mg II doublet we have used a Gaussian profile model (Salviander et al. 2007) with the initial guess of two Gaussian components for each line of the Mg II doublet; however, if the second component is not statistically required the procedure automatically drops it during the fit. The redshift and width of each component (narrow/broad) of Mg IIλ2796 were tied to the respective components of the Mg IIλ2803 line. The peak intensity of Mg IIλ2796 was constrained to be twice that of Mg IIλ2803, as is predicted theoretically.

In addition, we have constrained the width of the narrow component to be smaller than 1000 km s^{-1} and the width of the broader Mg II component to be same as the width of the UV Fe II emission line in the region (UV Fe II). We used an UV Fe II template generated by Tsuzuki et al. (2006), basically from the measurements of I ZW 1, which also employ calculations with the CLOUDY photoionization code (Ferland et al. 1998). This template is scaled and convolved to the FWHM value equivalent to the broad components of Mg II by taking into account the FWHM of the I ZW 1 template. The best-fitting value of the broad component of Mg II obtained in this way is finally used in our calculation of BH mass. To test for any overfitting caused by assuming two components, we also forced our procedure to fit only single components; however, in doing so for all our sources, a very good fit is never found for the wings of the lines nor for their central narrow cores.

(iii) Emission lines other than Fe II lines identified from the composite SDSS QSO spectrum (see table 2 in Vanden Berk et al. 2001) are modelled with single Gaussians.

The final fit is achieved by varying all free parameters simultaneously by minimizing the χ^2 value, until the reduced χ_r^2 is ≈ 1. Demonstrations of our spectral fitting in the UV region are given in Fig. 3 and values for FWHMs and EWs are given in Table 4.

4.3 Optical microvariability and spectral properties

The results from Paper I, with a modest sample of 37 sources, showed that the spectral properties for the sources with and without optical microvariability are quite similar. Here we search for better statistical results by adding our 46 new sources to the sample in Paper I. In these added 46 sources, among the 42 sources for which
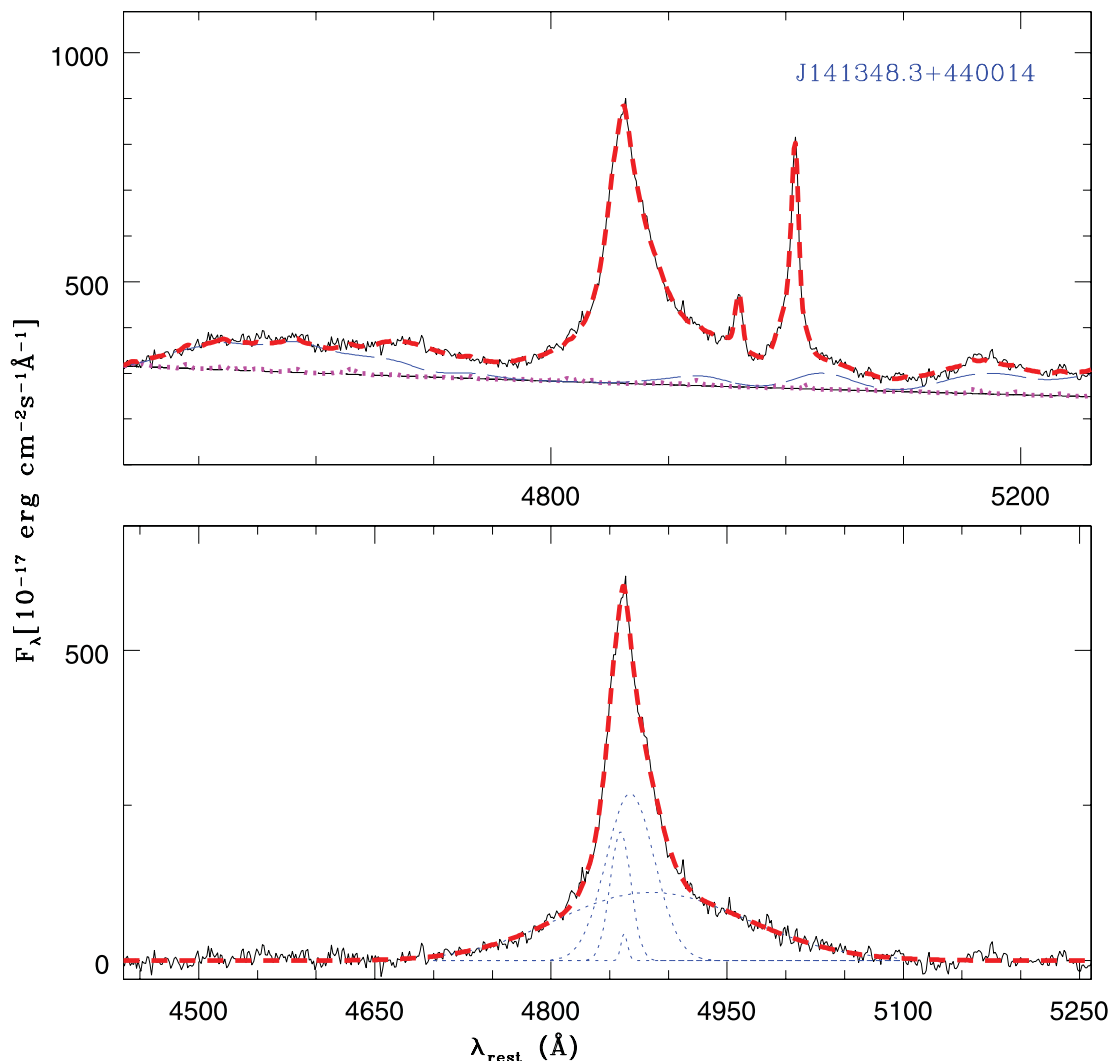
Figure 1. The best fit to the Hβ emission line of the IGO spectra of the QSO J141348.3+440014. Upper panel: complete spectrum fit (thick dashed/red) and components of the fit: power-law continuum (thin short-dashed/black line), broad Fe II (thin long-dashed/blue), narrow Fe II (dotted/magenta) lines. Lower panel: continuum, Fe II and metal-line subtracted spectrum (solid/black) with the best-fitting total Hβ profile (thick dashed/red) and Hβ components (dotted/blue) lines. Note that the entire fit is performed simultaneously (not first continuum subtraction then Hβ fit) but these aspects are shown separately for the sake of clarity.

we have spectral coverage of the Hβ line nine have shown optical microvariability while the other 33 have not been seen to show this property (Table 1). Of the four new sources with spectral coverage of the Mg II doublet, not one showed optical microvariability. We now investigate the correlation between spectral properties (i.e. FWHM and EW) and optical microvariability with our best-fitting values and with the larger combined sample of 83 sources. Among the 53 sources with only Hβ line coverage optical microvariability is shown by 15 sources, while of the 22 sources with only Mg II doublet spectral coverage only four have been shown to exhibit microvariability properties. Of the remaining eight source spectra that cover both Mg II and Hβ lines, optical microvariability was shown by one source.

From the multiple component fit of the Hβ line we have used the broad component fit (Section 4.1) to perform the comparison. This is because the clouds responsible for this broad component are clearly in the sphere of influence of the massive BH, while the other components may not be. In Fig. 4 we show the histograms of FWHM and rest-frame EW values based on our best fits for

Hβ and Mg II lines. The shaded and non-shaded regions correspond respectively to sources with and without confirmed optical microvariability. From these plots it appears that the distributions of sources with and without microvariability are on the whole quite similar. To quantify any differences in these distributions, we have performed Kolmogorov–Smirnov (KS) tests on all the distributions shown in Fig. 4. For the null hypothesis that the samples are drawn from similar distributions, we found the probabilities for the two Hβ(EW) distributions to be 0.90 and those for the two Mg II(EW) distributions to be 0.70. Similarly, we found the KS-test null probability value for the two Hβ(FWHM) distributions to be 0.29 and that for the two Mg II(FWHM) distributions to be 0.99.

In addition, in the 'blazar component' scenario, one would also expect some dilution of emission-line strength of the Fe II template for microvariable sources. To test this possibility, we have shown in Fig. 5 the EW distribution of the broad Fe II emission template for variable and non-variable sources, which by eye appear indistinguishable. The KS-test null probability value for these two Fe II distributions is 0.72 and so does not give
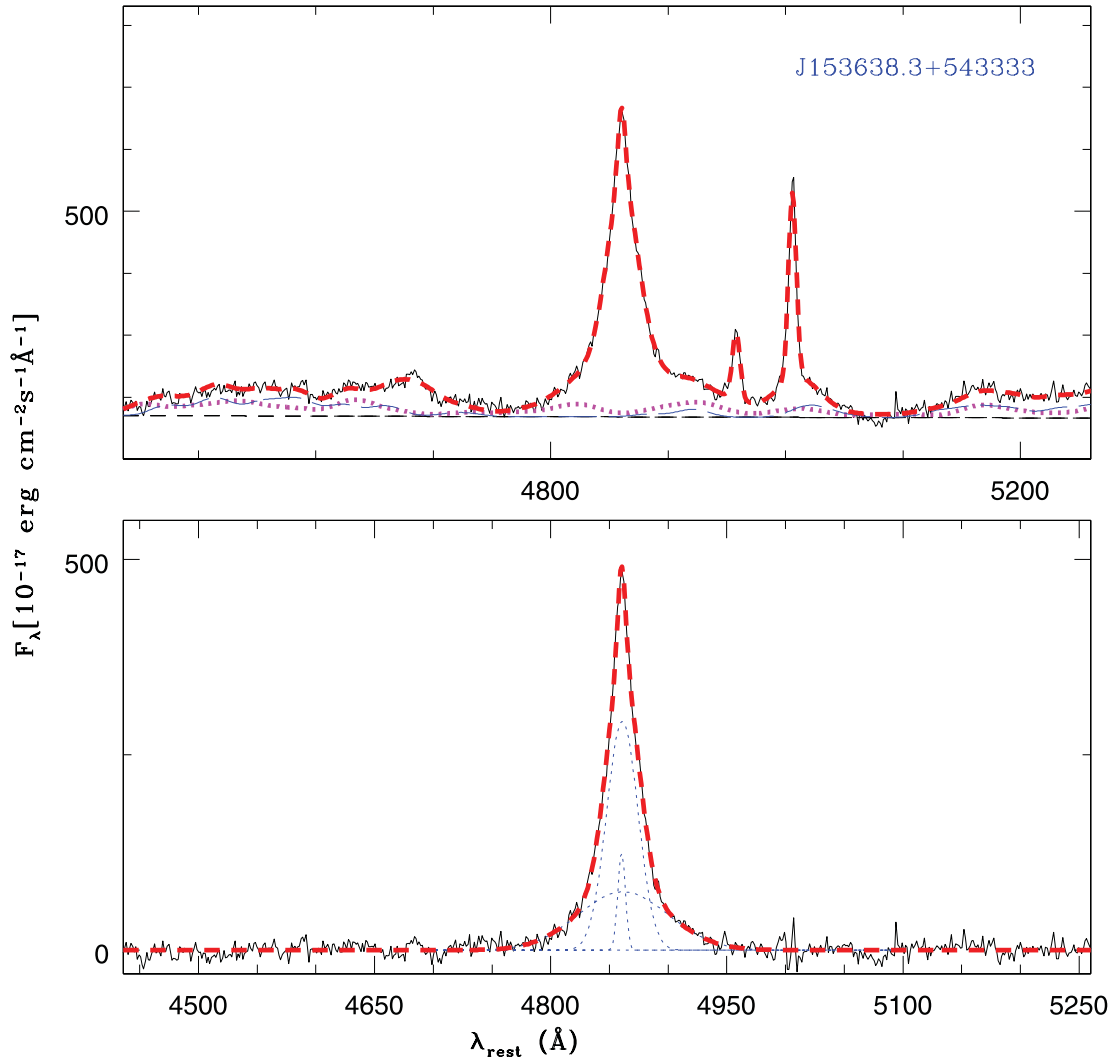
Figure 2. As in Fig. 1. IGO spectra for J153638.3+543333.

any hint of a blazar component. We have also tried to investigate the difference in the fraction of broad components of Hβ and Mg II and the respective total line intensity for sources with and without microvariability. We found that the distribution of this fraction of Hβ and Mg II broad components is quite similar for both variable and non-variable sources, as is shown in Fig. 6.

The above substantial null-hypothesis probabilities do not establish any relation of EW or FWHM with the optical microvariability properties and thus do not support a blazar-component model of microvariability for RQQSOs, which would predict smaller EW values for variable sources due to dilution of emission-line strength by jet components (Czerny et al. 2008). Here, the results drawn from a sample more than twice as large are in agreement with our results in Paper I.

5 BLACK HOLE MASS MEASUREMENTS, EDDINGTON RATIOS AND BLACK HOLE GROWTH TIMES

We have estimated the black hole masses using the virial single-epoch method (Dibai 1980), following the approach in Paper I.

This method has been shown to be consistent with reverberation-mapping masses (e.g. Bochkarev & Gaskell 2009). Improved empirical relationships (e.g. Vestergaard & Peterson 2006) are used for estimating the central BH mass based on FWHMs of emission lines such as Hβ and Mg II. We used equations (1) and (2) in Paper I, taken from Vestergaard & Peterson (2006) and McLure & Dunlop (2004), to determine respectively the black hole masses based on Hβ lines and Mg II lines, namely

$$\log M_{\text{BH}}(\text{H}\beta) = \log\left[\left(\frac{\text{FWHM}(\text{H}\beta)}{1000\,\text{km s}^{-1}}\right)^2\right] + (6.91 \pm 0.02)$$
$$+ \log\left(\frac{\lambda L_\lambda(5100\,\text{Å})}{10^{44}\,\text{erg s}^{-1}}\right)^{0.50\pm0.06}, \quad (1)$$

$$\log M_{\text{BH}}(\text{Mg II}) = (0.62 \pm 0.14)\log\left(\frac{\lambda L_\lambda(3000\,\text{Å})}{10^{44}\,\text{erg s}^{-1}}\right)$$
$$+ 2\log\left(\frac{\text{FWHM}(\text{Mg II})}{\text{km s}^{-1}}\right) + 0.505, \quad (2)$$

where $L_\lambda(5100\,\text{Å})$ and $L_\lambda(3000\,\text{Å})$ are the monochromatic luminosity at 5100 Å and 3000 Å, respectively, which we have computed

Table 3. Results of the Hβ line analysis.

QSO Name	$z_{\rm emi}$	$\frac{L(5100\,\text{Å})}{10^{43}\,{\rm erg\,s^{-1}}}$	FWHM (km s^{-1})	$\log(\frac{M_{\rm bh}}{M_\odot})$	$\frac{L_{\rm bol}}{L_{\rm edd}}$	EW$_B$ (Å)	EW$_{\rm all}$ (Å)
J000619.5+201210	0.0262	5.16	3292.99	7.80	0.06	54.10	113.68 ± 0.33
J002913.6+131603	0.1462	150.94	3615.62	8.62	0.25	17.30	36.56 ± 0.31
J004547.3+041024	0.3825	373.16	3025.37	8.66	0.55	31.97	65.59 ± 0.53
J005334.9+124136	0.0604	28.55	2095.22	7.78	0.32	31.49	58.97 ± 0.32
J005452.1+252538	0.1651	63.57	4272.75	8.57	0.11	54.00	119.86 ± 0.62
J011354.5+390744	0.2325	16.18	4179.08	8.26	0.06	46.60	84.73 ± 1.18
J012240.6+231015	0.0528	3.77	3136.91	7.69	0.05	0.93	37.37 ± 0.49
J051611.4−000859	0.0334	9.91	1654.62	7.35	0.30	3.48	118.20 ± 0.22
J051633.4−002713	0.2922	131.20	3959.10	8.66	0.19	61.56	105.36 ± 0.48
J055453.6+462622	0.0245	1.35	1882.71	7.03	0.09	24.15	158.56 ± 0.59
J071415.1+454156	0.0560	7.97	3822.48	8.03	0.05	42.88	115.60 ± 0.51
J073657.0+584613	0.0392	5.62	2868.64	7.70	0.08	39.24	94.99 ± 0.41
J084742.4+344504	0.0640	25.27	2406.85	7.87	0.23	4.87	66.98 ± 0.27
J092512.9+521711	0.0355	1.06	2657.45	7.27	0.04	53.63	121.19 ± 0.63
J092603.3+124404	0.0289	2.34	2024.97	7.21	0.10	18.53	102.05 ± 0.47
J095652.4+411522	0.2334	395.74	7136.27	9.42	0.10	47.62	87.21 ± 0.36
J101420.7−041840	0.0582	5.26	2180.48	7.45	0.13	16.03	35.17 ± 0.61
J105143.9+335927	0.1671	29.00	5980.04	8.69	0.04	7.75	102.03 ± 0.76
J110631.8−005252	0.4232	185.83	2465.65	8.33	0.59	54.71	100.49 ± 0.68
J111908.7+211918	0.1759	67.27	3197.73	8.33	0.21	83.05	201.91 ± 0.72
J112147.1+114418	0.0500	10.33	2322.45	7.65	0.16	33.37	66.36 ± 0.35
J112302.3−273004	0.3902	271.41	5058.81	9.03	0.17	64.23	67.93 ± 0.47
J112439.2+420145	0.2243	97.42	3519.45	8.50	0.21	2.34	87.53 ± 0.54
J115349.3+112830	0.1763	46.83	4711.23	8.59	0.08	58.22	105.72 ± 0.59
J120309.6+443153	0.0017	0.01	1617.19	5.84	0.01	18.63	28.88 ± 1.20
J121032.6+392421	0.0032	0.34	1997.36	6.78	0.04	22.95	81.20 ± 0.17
J132349.5+654148	0.1677	46.77	2857.81	8.16	0.22	40.22	73.15 ± 0.65
J140516.2+255534	0.1651	50.57	1912.69	7.83	0.51	45.00	73.82 ± 0.49
J141348.3+440014	0.0897	26.76	2923.47	8.06	0.16	48.78	139.40 ± 0.70
J141700.7+445606	0.1475	16.46	1534.52	7.39	0.45	2.79	35.01 ± 0.63
J142906.6+011706	0.0866	8.55	3100.99	7.86	0.08	19.46	108.65 ± 0.85
J144207.4+352623	0.0772	17.34	1723.99	7.50	0.37	40.97	62.95 ± 0.51
J153638.3+543333	0.0387	2.93	1918.30	7.21	0.12	54.76	99.34 ± 0.69
J155202.3+201402	0.2518	25.79	2108.52	7.76	0.30	56.78	111.97 ± 1.06
J162011.3+172428	0.1145	18.14	3814.02	8.20	0.08	13.63	52.06 ± 0.99
J170124.8+514920	0.2914	358.12	2656.36	8.54	0.71	23.23	35.43 ± 1.70
J175116.6+504539	0.2974	149.87	2484.15	8.29	0.52	40.79	78.44 ± 0.41
J211452.6+060742	0.4850	778.92	3695.78	8.99	0.54	73.60	81.17 ± 0.53
J213227.8+100819	0.0629	19.10	2870.28	7.97	0.14	57.01	104.75 ± 1.60
J221712.2+141421	0.0655	22.58	5499.40	8.57	0.04	77.21	93.63 ± 1.55
J230315.6+085226	0.0158	3.68	1888.66	7.24	0.14	22.62	70.39 ± 0.84
J230702.9+043257	0.0470	1.68	1667.88	6.97	0.12	8.19	87.64 ± 1.31

from the best-fitting power-law continuum, $a_1\lambda^{-\alpha}$, in our simultaneous fit of the whole spectral region.

We have also estimated the Eddington ratio $\ell \equiv L_{\rm bol}/L_{\rm edd}$, where $L_{\rm bol}$ is taken as $5.9 \times \lambda L_\lambda(3000\,\text{Å})$ and $9.8 \times \lambda L_\lambda(5100\,\text{Å})$ for Mg II and Hβ, respectively (McLure & Dunlop 2004) and $L_{\rm edd} = 1.45 \times 10^{38}(M_{\rm bh}/M_\odot)\,{\rm erg\,s^{-1}}$, assuming a mixture of hydrogen and helium so that the mean molecular weight is $\mu = 1.15$. The combined sample results are given in Fig. 7, which by eye indicates that distributions of sources with and without optical microvariability appear similar with respect to both BH mass and ℓ. Quantitatively, this is also supported by KS tests, which show that the probability of the null hypothesis ($P_{\rm null}$) for sources with and without microvariation, is as high as 0.69 for BH mass distributions and 0.11 for Eddington ratio (ℓ) distributions based on Hβ lines fit. Similarly using Mg II lines, the null hypothesis ($P_{\rm null}$) for sources with and without microvariation is as high as 0.98 for BH mass distributions and 0.94 for Eddington ratio (ℓ) distributions.

To test the reasonableness of the estimated Eddington ratios, we also computed black hole growth times to compare them with the age of the Universe (at the time the QSO is observed) by using the following equation (Dietrich et al. 2009):

$$M_{\rm bh}(t_{\rm obs}) = M_{\rm bh}^{\rm seed}(t_0)\exp\left(\ell\,\frac{(1-\epsilon)}{\epsilon}\,\frac{\tau}{t_{\rm edd}}\right), \tag{3}$$

where $\tau = t_{\rm obs} - t_0$ is the time elapsed between the initial time t_0 and the observed time $t_{\rm obs}$, $M_{\rm bh}^{\rm seed}$ is the seed BH mass, ϵ is the efficiency of conversion of mass to energy in the accretion flow and $t_{\rm edd}$ is the Eddington time-scale, with $t_{\rm edd} = \sigma_{\rm T}c/(4\pi Gm_{\rm p}) = 3.92 \times 10^8$ yr (Rees 1984). We used equation (3) to derive the times, τ, necessary to accumulate the BH masses listed in Tables 3 and 4 for seed black holes with masses of $M_{\rm bh}^{\rm seed} = 10\,M_\odot$, $10^3\,M_\odot$ and $10^5\,M_\odot$, respectively. Two cases are considered: (i) BHs are accreting at the Eddington limit, i.e. $\ell = L_{\rm bol}/L_{\rm edd} = 1.0$ and the efficiency of converting mass into energy is $\epsilon = 0.1$, and (ii) BHs are accreting
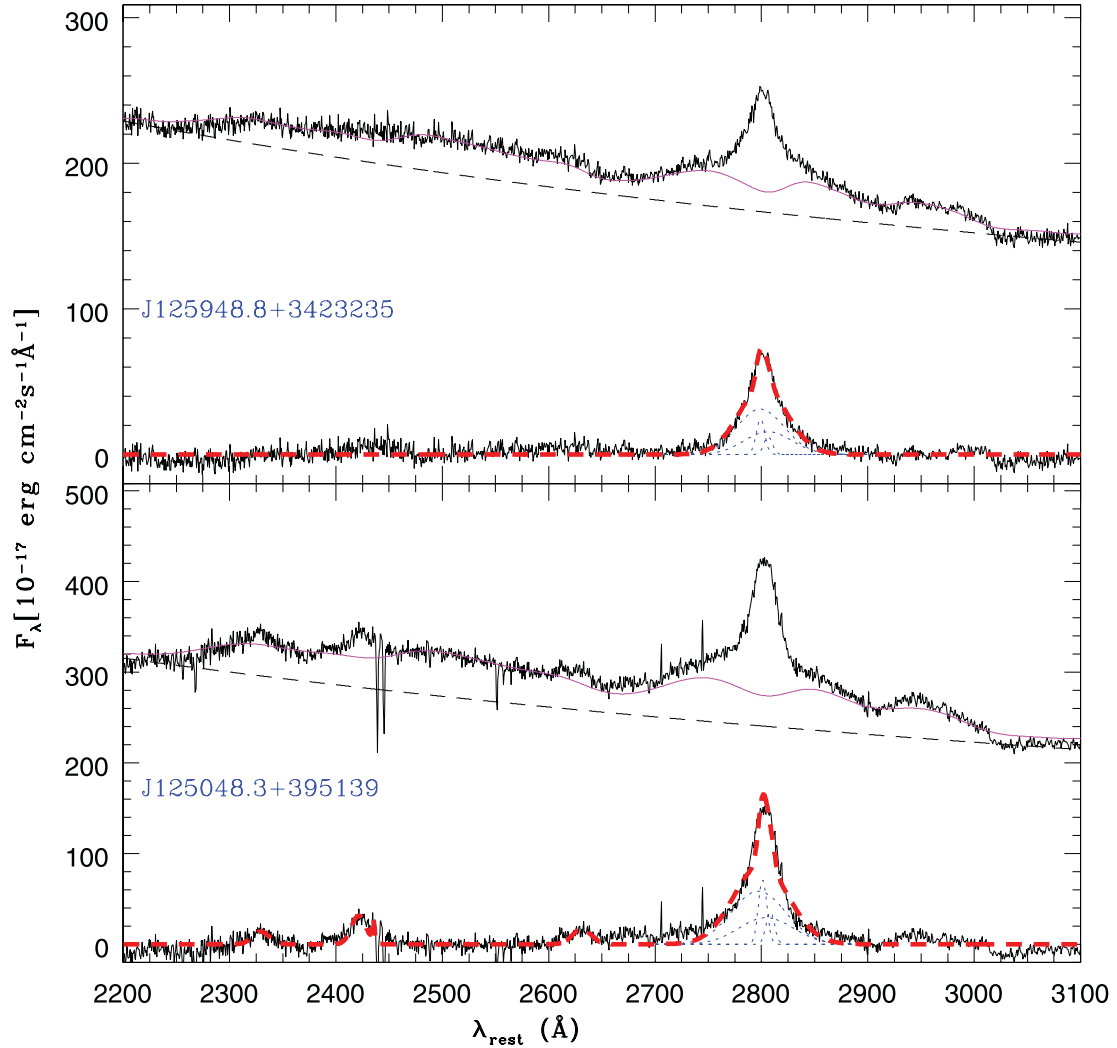
Figure 3. Mg II emission-line fits for two RQQSOs, J125948.8+342323.5 and J125048.3+395139. The upper plot in each panel shows the SDSS spectra and continuum as a dashed line with the best-fitting UV Fe II template as a solid (magenta) line. The lower plot in each panel shows the continuum and Fe II subtracted spectrum (solid), the best-fitting Mg II profile (thick dashed/red) and Mg II $\lambda\lambda$2796,2803 components by (dotted/blue) lines. Note that the entire fits are performed simultaneously (not first continuum subtraction, then Mg II fit) but are shown separately for the sake of clarity.

with our observed Eddington ratios and $\epsilon = 0.1$. These results are summarized in Tables 5 and 6, showing that the key criterion that black hole growth time should be smaller than the age of Universe is fulfilled for all sources.

In our Paper I we found a weak negative correlation between the Hβ EW and the Eddington ratio, ℓ and a significant one between the Mg II EW and ℓ. In Fig. 8 we show the observed variations of FWHM and EW with ℓ based on both Hβ and Mg II lines for our combined sample. There appear to be linear relations of both

FWHM and EW with ℓ in these log–log plots. For the FWHM plots this is unsurprising, since the BH masses are proportional to L_{edd}. To quantify any such linear relations for the EW plots we perform linear regressions, treating ℓ as the independent variable, and find

$$\log EW(H\beta) = (1.33 \pm 0.12) + (-0.05 \pm 0.13)\log(\ell),$$
$$\log EW(Mg\ II) = (1.07 \pm 0.04) + (-0.29 \pm 0.10)\log(\ell). \qquad (4)$$

Here the errors in the fit parameters are purely statistical. We have calculated the Spearman rank correlations of log EW with log ℓ and

Table 4. Results of the Mg II line analysis.

QSO Name	z_{emi}	$\frac{L(3000\,\text{Å})}{10^{43}\,\text{erg s}^{-1}}$	FWHM (km s^{-1})	$\log(\frac{M_{bh}}{M_\odot})^a$	$\log(\frac{M_{bh}}{M_\odot})^b$	$\frac{L_{bol}}{L_{edd}}$	EW$_B$ (Å)	EW$_{all}$ (Å)
J112731.9−304446	0.6679	5691.58	1447.36	8.53	9.00	2.32	13.14	13.14 ± 0.63
J125048.3+395139	1.0318	1294.13	3029.19	8.78	9.32	0.25	19.64	23.46 ± 0.31
J125948.8+342323	1.3762	2577.21	3297.04	9.04	9.54	0.30	14.12	16.28 ± 0.27
J135458.7+005211	1.1253	1451.56	3007.11	8.80	9.34	0.27	22.30	26.21 ± 0.17

^{a}Using the McLure & Dunlop (2004) scaling relation, i.e. equation (2).
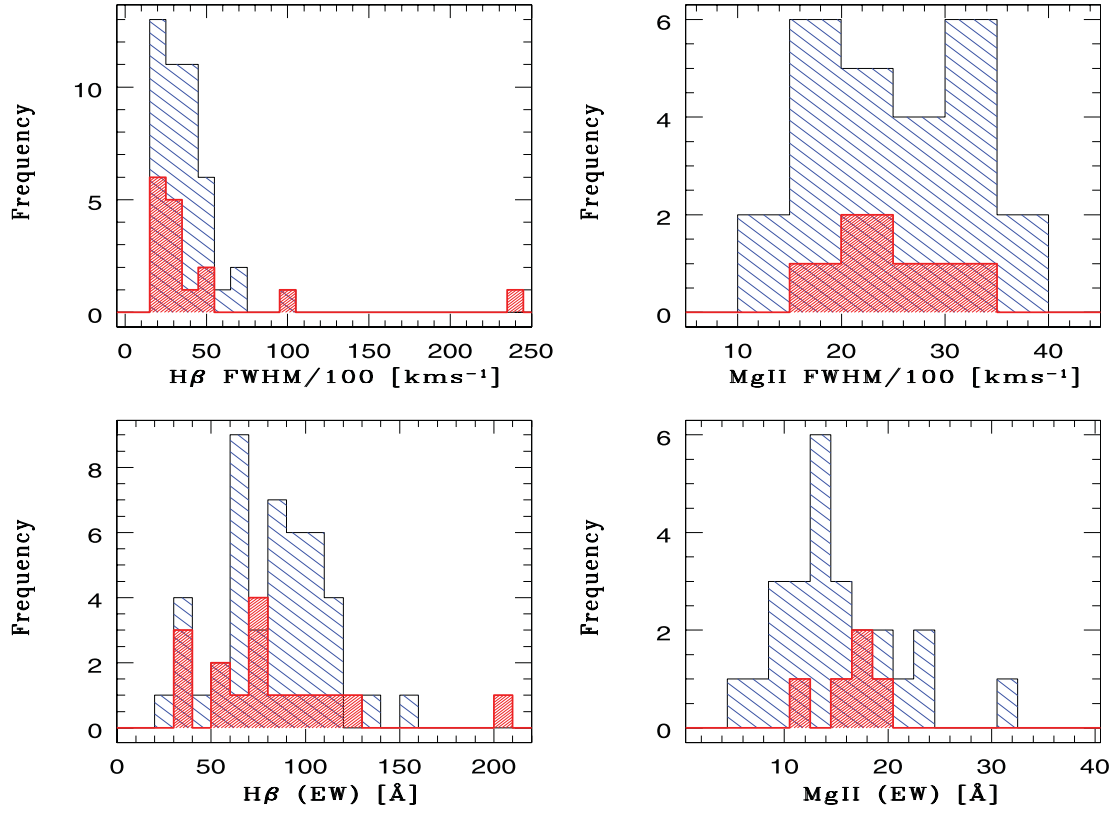^{b}Using the fixed slope of the $r - L$ relation from Dietrich et al. (2009), their equation (6).

Figure 4. Histograms of FWHM and rest-frame equivalent width (EW) based on best fits of Hβ and Mg II lines. The red (dark) shaded regions correspond to sources with confirmed optical microvariability while the striped regions correspond to those sources for which optical microvariability has not been detected.
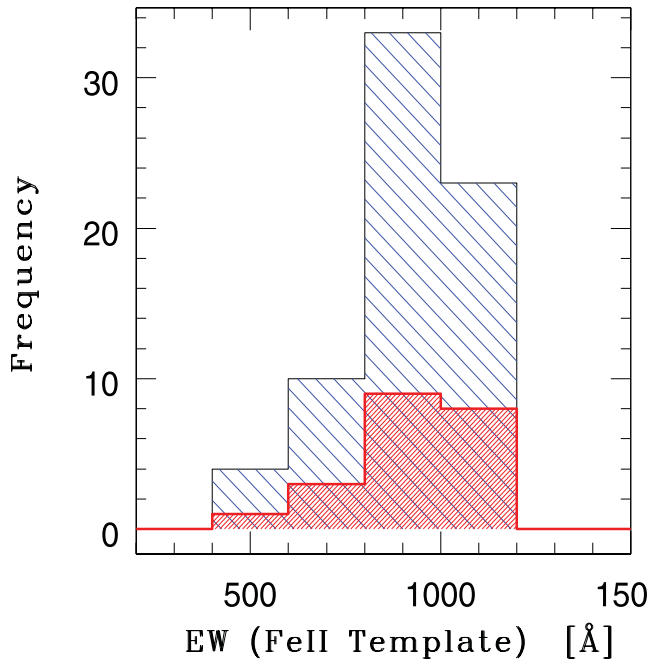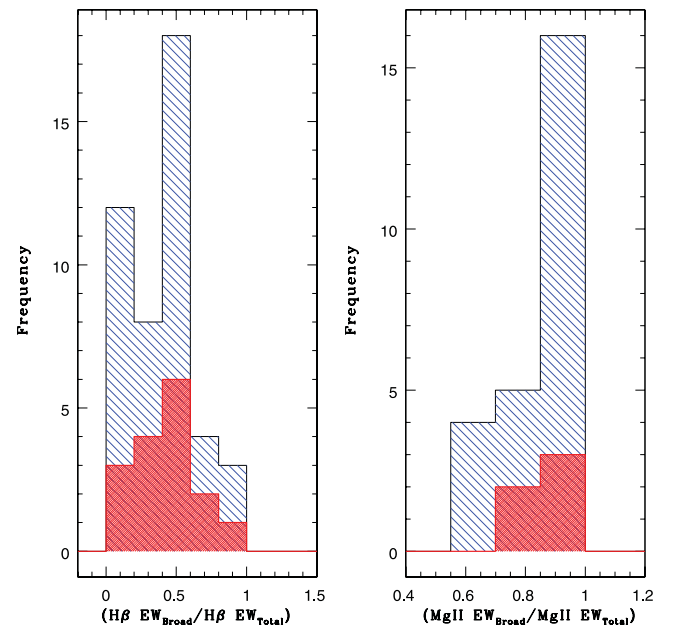

Figure 5. Histograms of EW of broad Fe II template. The red (dark) shaded regions correspond to sources with confirmed optical microvariability while the striped regions correspond to those sources for which optical microvariability has not been detected.

Figure 6. The left panel shows histograms of the fraction of the broad Hβ component in Hβ emission lines and the right panel shows the broad Mg II component fraction in Mg II emission lines.
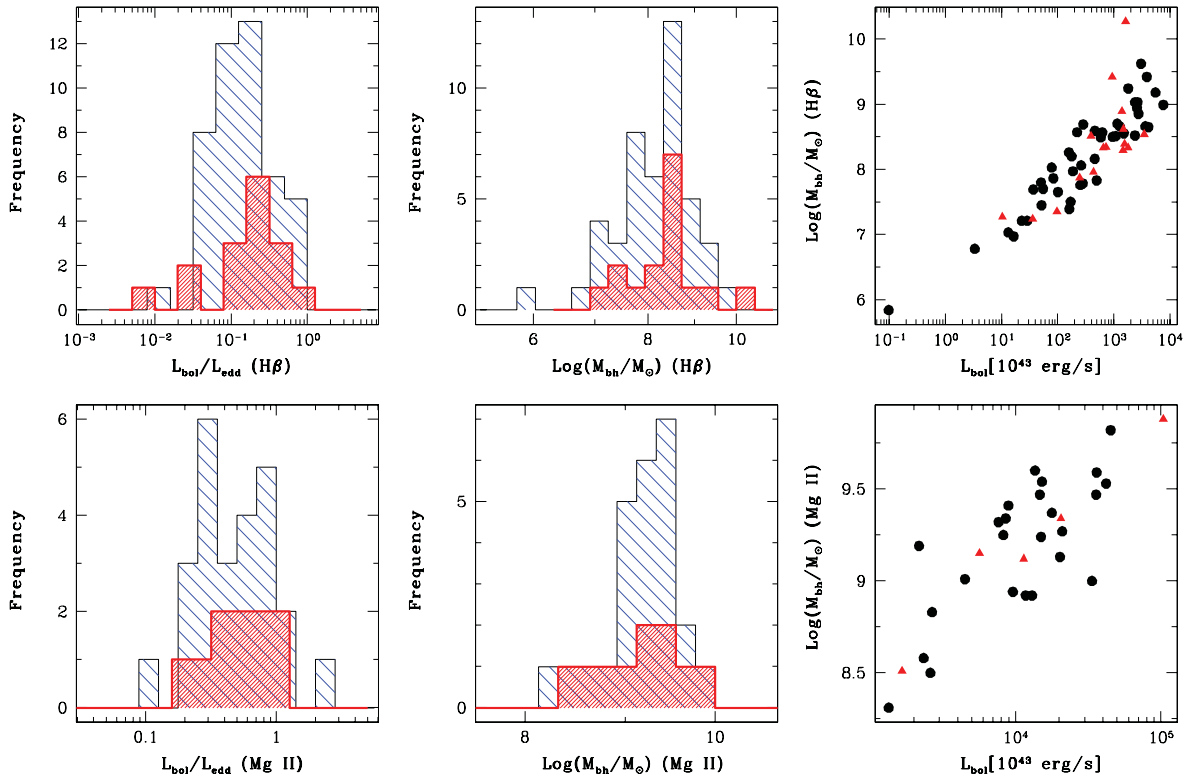
Figure 7. The upper left and middle panels show histograms of Eddington ratio L_{bol}/L_{edd} and $\log(M_{bh}/M_{\odot})$ based on the $H\beta$ line, while the corresponding bottom panels show results based on the Mg II line. The shaded regions correspond to sources with confirmed optical microvariability, while the non-shaded regions are for those sources for which optical microvariability is not detected. The right upper and bottom panels respectively show plots of $\log(M_{bh}/M_{\odot})$ versus L_{bol}. Triangles and circles respectively show sources with and without confirmed optical microvariability.

found the correlation coefficient for $r_s(H\beta) = -0.05$, with null probability $p_{null} = 0.72$, and so no significant correlation is present, whereas $r_s(Mg\,II) = -0.45$, with $p_{null} = 0.013$, and so this negative correlation is significant. These results are in agreement with those from Paper I, which were based on a modest sample size.

6 DISCUSSION AND CONCLUSIONS

Modern surveys such as SDSS have allowed investigators to carry out spectral analyses of large numbers of quasars to estimate central BH masses using virial approaches (e.g. Fine et al. 2008; Shen et al. 2008; Vestergaard & Osmer 2009) and to understand their demography (Dong et al. 2009, 2011). These studies have resulted in very important insights into the important physical parameters of AGN central engines and their environments.

Dong et al. (2009) found that the variation of the emission-line strength in AGNs is regulated by ℓ, presumably because it governs the global distributions of properties such as the column density of clouds gravitationally bound in the line-emitting region. Shen et al. (2008) have found that the line widths of $H\beta$ and Mg II follow log-normal distributions with very weak dependences on redshift and luminosity. Fine et al. (2008) used Mg II lines to estimate BH masses and found that the scatter in measured BH masses is luminosity-dependent, showing less scatter for more luminous objects.

The sample we have considered more than doubles our sample in Paper I, but still is much smaller than those in the above papers, which consist of between 1100 and almost 57 700 quasars. However, each member in our sample has been carefully selected to be among the special group of RQQSOs and Seyfert galaxies already examined for optical microvariability (e.g. Carini et al. 2007). This

criterion demands that modest aperture (usually 1–2 m) telescopes can make precise photometric measurements in just a few minutes, and so limits the members to those rare QSOs with bright apparent magnitudes (usually $m_V < 17.5$). In addition, we have taken special care in the fitting of the line profiles, as discussed in Sections 4.1 and 4.2.

It has been found that for BL Lacertae objects the emission-line detection and strength varies with overall continuum flux (e.g. Nilsson et al. 2008). For instance, when BL Lacs are in optically faint states, weak emission lines have sometimes been detected that are usually not seen during their high states, presumably due to their being swamped by the Doppler-boosted continuum arising in strong jet components (Nilsson et al. 2009).

To check whether the continuum states of our objects, high (bright) or low (faint), have any such effect on their spectral properties, we have searched in the SDSS DR8 archive for multi-epoch photometric and spectroscopic observations for the 44 SDSS sources in our sample. We found that multi-epoch photometric fluxes were available for 14 sources, with time gaps ranging from a few days to years. We then searched for spectroscopic observations of these sources and found that multi-epoch spectra are available only for three sources, namely J025937.46+003736.3, J084030.0+465113 and J093502.6+433111. Among them, J093502.6+433111 has two spectra with roughly a one-year time gap (observations on 2002 February 20 and 2003 January 31) but only a single photometric data point at all close to either of those dates (2001 December 20). For J084030.0+465113 two spectra were available about a month apart (2001 January 13 and 2001 February 19) but these had their two closest photometric observations made on 2001 January 24 and

Table 5. BH growth time estimates (in units of Gyr) from the Hβ line analysis.

Object	z_{emi}	Black hole growth time-scale						Age of the Universe (at z_{emi}) [10^9 yr]
		$L_{bol}/L_{edd} = 1.0$ M_{bh}(seed)			L_{bol}/L_{edd} obs.[a] M_{bh}(seed)			
		$10\,M_\odot$	$10^3\,M_\odot$	$10^5\,M_\odot$	$10\,M_\odot$	$10^3\,M_\odot$	$10^5\,M_\odot$	
J000619.5+201210	0.0262	0.68	0.48	0.28	12.40	8.75	5.11	13.11
J002913.6+131603	0.1462	0.76	0.56	0.36	3.09	2.28	1.47	11.62
J004547.3+041024	0.3825	0.77	0.57	0.37	1.38	1.02	0.66	9.33
J005334.9+124136	0.0604	0.68	0.48	0.28	2.12	1.50	0.87	12.66
J005452.1+252538	0.1651	0.76	0.56	0.36	6.60	4.86	3.11	11.41
J011354.5+390744	0.2325	0.73	0.53	0.33	11.94	8.65	5.36	10.70
J012240.6+231015	0.0528	0.67	0.47	0.27	12.90	9.05	5.19	12.76
J051611.4−000859	0.0334	0.64	0.44	0.24	2.11	1.44	0.78	13.01
J051633.4−002713	0.2922	0.77	0.57	0.37	4.00	2.96	1.91	10.12
J055453.6+462622	0.0245	0.60	0.40	0.20	7.03	4.70	2.37	13.13
J071415.1+454156	0.0560	0.71	0.50	0.30	13.82	9.89	5.96	12.71
J073657.0+584613	0.0392	0.67	0.47	0.27	8.84	6.20	3.56	12.93
J084742.4+344504	0.0640	0.69	0.49	0.29	3.02	2.14	1.26	12.61
J092512.9+521711	0.0355	0.63	0.43	0.23	16.55	11.27	5.99	12.98
J092603.3+124404	0.0289	0.62	0.42	0.22	6.36	4.31	2.26	13.07
J095652.4+411522	0.2334	0.84	0.64	0.44	8.20	6.25	4.30	10.69
J101420.7−041840	0.0582	0.65	0.45	0.25	5.09	3.51	1.93	12.69
J105143.9+335927	0.1671	0.77	0.57	0.37	19.28	14.27	9.25	11.39
J110631.8−005252	0.4232	0.74	0.53	0.33	1.25	0.91	0.57	9.00
J111908.7+211918	0.1759	0.74	0.53	0.33	3.48	2.53	1.58	11.29
J112147.1+114418	0.0500	0.67	0.47	0.27	4.25	2.97	1.69	12.79
J112302.3−273004	0.3902	0.81	0.60	0.40	4.77	3.58	2.39	9.26
J112439.2+420145	0.2243	0.75	0.55	0.35	3.58	2.63	1.67	10.78
J115349.3+112830	0.1763	0.76	0.56	0.36	9.40	6.92	4.44	11.29
J120309.6+443153	0.0017	0.49	0.28	0.08	48.54	28.48	8.42	13.44
J121032.6+392421	0.0032	0.58	0.38	0.18	14.86	9.72	4.58	13.42
J132349.5+654148	0.1677	0.72	0.52	0.32	3.26	2.35	1.44	11.38
J140516.2+255534	0.1651	0.68	0.48	0.28	1.34	0.95	0.56	11.41
J141348.3+440014	0.0897	0.71	0.51	0.31	4.45	3.19	1.93	12.29
J141700.7+445606	0.1475	0.64	0.44	0.24	1.41	0.97	0.53	11.61
J142906.6+011706	0.0866	0.69	0.49	0.29	8.60	6.09	3.59	12.33
J144207.4+352623	0.0772	0.65	0.45	0.25	1.77	1.23	0.68	12.45
J153638.3+543333	0.0387	0.62	0.42	0.22	5.10	3.46	1.82	12.94
J155202.3+201402	0.2518	0.68	0.48	0.28	2.26	1.59	0.92	10.51
J162011.3+172428	0.1145	0.72	0.52	0.32	9.38	6.77	4.17	11.99
J170124.8+514920	0.2914	0.76	0.56	0.36	1.07	0.79	0.50	10.13
J175116.6+504539	0.2974	0.73	0.53	0.33	1.40	1.02	0.63	10.07
J211452.6+060742	0.4850	0.80	0.60	0.40	1.49	1.12	0.75	8.53
J213227.8+100819	0.0629	0.70	0.50	0.30	5.03	3.59	2.14	12.63
J221712.2+141421	0.0655	0.76	0.56	0.36	18.52	13.62	8.73	12.59
J230315.6+085226	0.0158	0.63	0.43	0.22	4.44	3.02	1.59	13.25
J230702.9+043257	0.0470	0.60	0.40	0.20	4.87	3.24	1.61	12.83

[a]Values of ℓ estimated using Hβ lines (Table 3).

Table 6. BH growth time estimates (in units of Gyr) from the Mg II line analysis.

| Object	z_{emi}	Black hole growth time-scale						Age of the Universe (at z_{emi}) [10^9 yr]
		$L_{bol}/L_{edd} = 1.0$ M_{bh}(seed)			L_{bol}/L_{edd} obs.[a] M_{bh}(seed)			
		$10\,M_\odot$	$10^3\,M_\odot$	$10^5\,M_\odot$	$10\,M_\odot$	$10^3\,M_\odot$	$10^5\,M_\odot$	
J112731.9−304446	0.6679	0.80	0.60	0.40	0.35	0.26	0.17	7.35
J125048.3+395139	1.0318	0.83	0.63	0.43	3.34	2.54	1.73	5.63
J125948.8+342323	1.3762	0.86	0.66	0.46	2.85	2.19	1.52	4.52
J135458.7+005211	1.1253	0.84	0.64	0.44	3.10	2.35	1.61	5.29

[a]Values of ℓ estimated using Mg II lines (Table 4).
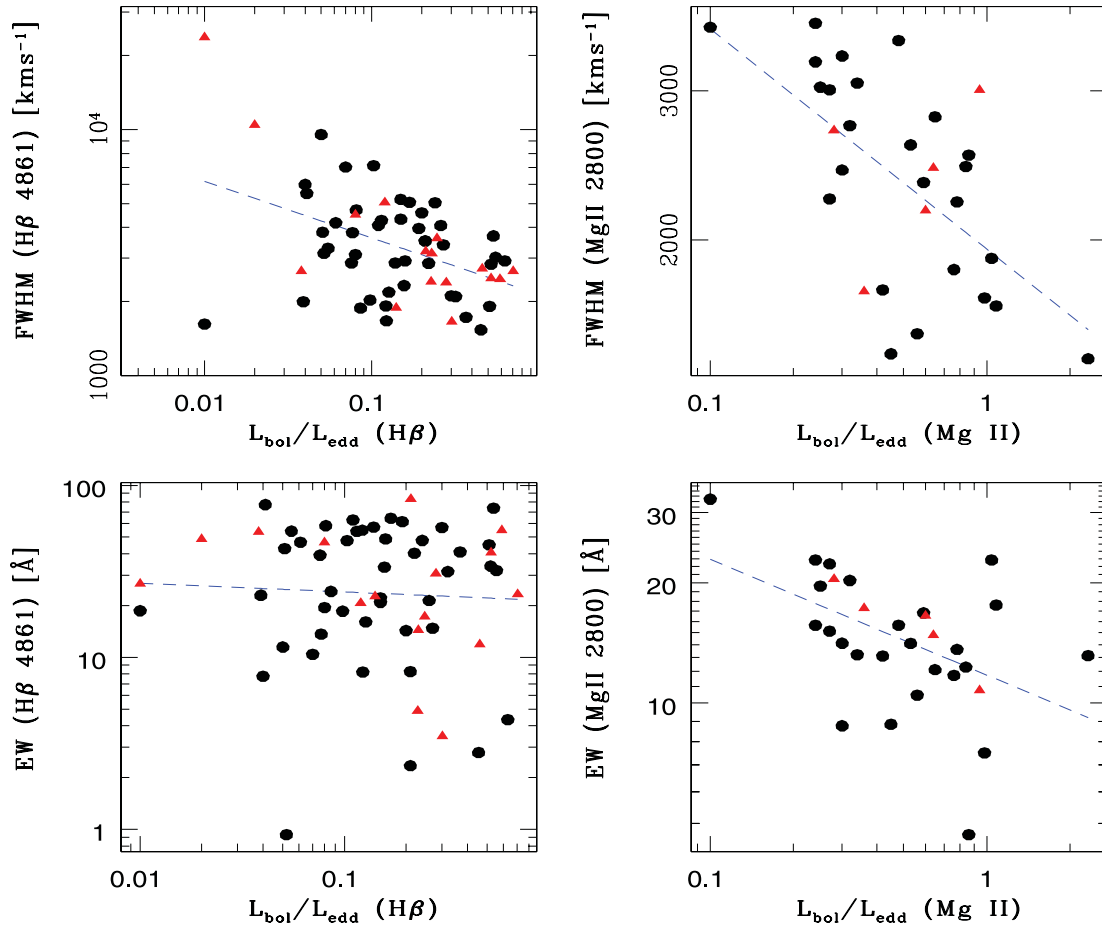
Figure 8. Observed variation of FWHM (upper) and EW (lower) with Eddington ratio ($\ell = L_{bol}/L_{edd}$) based on both Hβ (left) and Mg II (right) lines. Triangles and circles respectively show sources with and without confirmed optical microvariability. The dashed lines show the linear regression fits treating ℓ as the independent variable. The correlations of both FWHM and EW with ℓ suggest that the Eddington ratio is one of the fundamental parameters responsible for some AGN properties.

2001 January 26, respectively. As these two photometric observations have only a two-day time gap and have a g-magnitude difference of only 0.01, this object also does not serve to test for such a correlation. We are left with just one source, J025937.46+003736.3, that has both photometric and spectroscopic multi-epoch data that are well paired. For this source there were two spectral observations on 2000 November 25 and 2001 September 21 and corresponding photometric observations on 2000 November 27 and 2001 September 21 with g magnitudes of 16.41 and 16.47, respectively. As this g-magnitude difference of 0.06 is much larger than the typical RQQSO INOV magnitude variation of about 0.01 mag over a night, this source is the only one that might test whether brighter or fainter states have any significant effect on spectral properties. Even though this difference in brightness is modest, we carried out our spectral fits to each of the two spectra to estimate the FWHMs and EWs of the Hβ line, using the same method as for other sources (Section 4.1). The best-fitting EW(Hβ) of the broad component for the first epoch was found to be 30.47 ± 0.63 Å and that for second epoch 29.23 ± 0.45 Å. These values are statistically indistinguishable, so there is no evidence for any effect due to variation in source brightness. However, in order to say anything firm about this possibility for RQQSOs, nearly simultaneous spectroscopic and photometric measurements would need to be made on at least two occasions for a decent-sized sample.

In this paper we continued our work begun in Paper I with 37 RQQSOs by analysing spectra for an additional 46 sources. Most of these spectra were obtained by us at the IGO. We conclude that there is a significant negative correlation between Mg II EW and ℓ (Fig. 8; Section 5), as also found in Paper I (fig. 7 of that paper) and by Dong et al. (2009). However, we have not found any significant correlation between the equivalent widths of the Hβ lines and the Eddington ratio ℓ. We can also see from Fig. 8 that there is a decline in FWHM with ℓ; this is not surprising, since the BH masses are proportional to L_{edd}. In Paper I (fig. 8), we noticed an interesting tendency for sources with detectable optical microvariability to have somewhat lower luminosity than those with no such detections, which required investigation with a larger sample. One might expect such a trend, as lower mass BHs would have correspondingly shorter physical time-scales. However, as can be seen from Fig. 9 there is no such trend seen with our new larger sample of microvariable sources (16 as compared to 7 in Paper I).

We also find that the BH masses estimated from the FWHMs of both the Hβ and Mg II lines are reasonable, in that growth to their estimated masses from even small seed BHs is easily possible within the age of the Universe at their observed redshift if the mean ℓ values are close to unity (Tables 5 and 6). This remains true for the great majority of RQQSOs, even if the value of ℓ we compute from the current continuum flux is constant until the time we observe
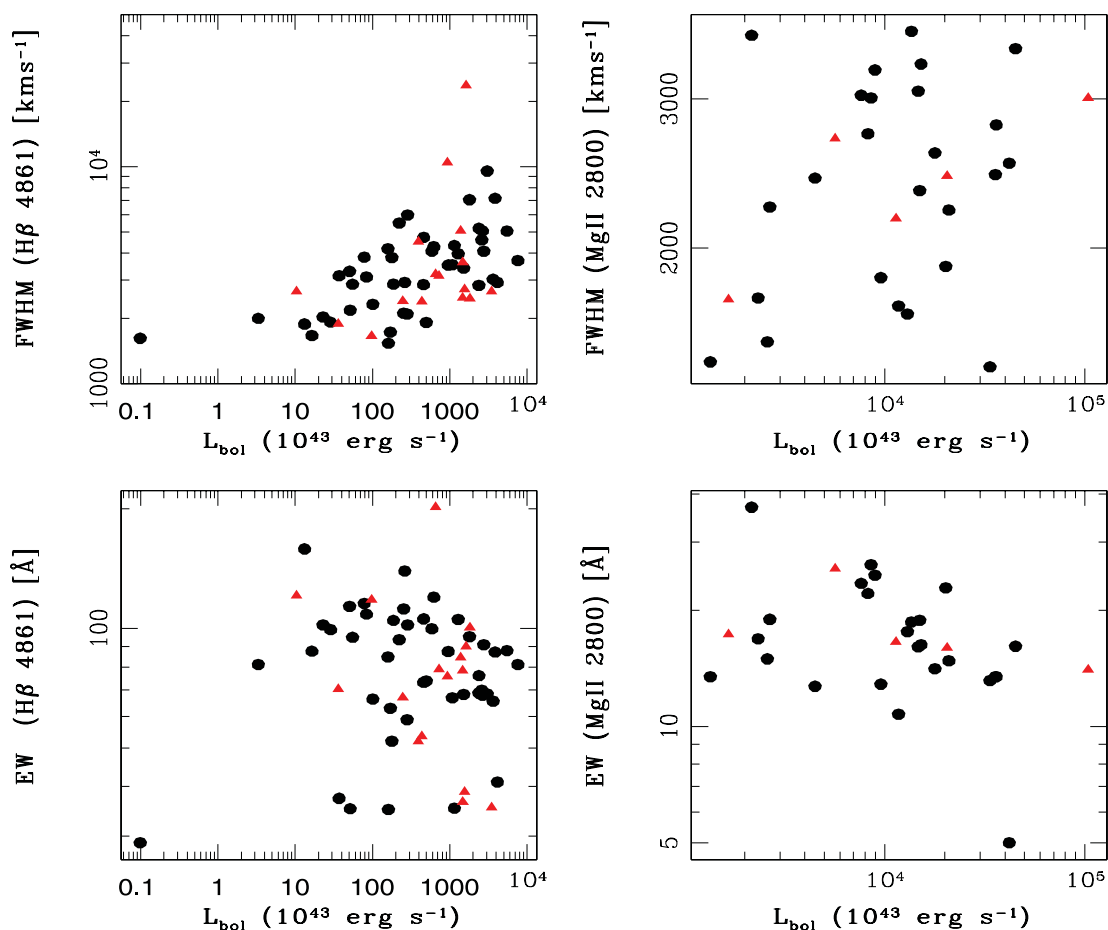
Figure 9. As in Fig. 8 with L_{bol} as the independent variable. This panel indicates that sources with and without optical microvariability are similar in luminosity.

them; however, this assumption does not work for eight out of the 42 QSOs with Hβ lines while we consider $M_{bh}(\text{seed}) = 10\,M_\odot$, for four while we consider $M_{bh}(\text{seed}) = 10^3\,M_\odot$ and for none while we consider $M_{bh}(\text{seed}) = 10^5\,M_\odot$, suggesting that in a few cases $M_{bh}(\text{seed})$ might need to be as large as $10^5\,M_\odot$ or else the accretion rate was substantially higher in the past. With Mg II line profiles, no QSO was found problematic with respect to this assumption (Table 6).

As Fig. 4 shows, histograms of FWHM and rest-frame EW values for sources with and without confirmed optical microvariability are on the whole quite similar. Under the null hypothesis that the samples are drawn from a similar distribution, using KS tests we find a probability of 0.90 for the Hβ(EW) distributions and 0.70 for the Mg II(EW) distributions. Similarly, this null probability for the FWHM distributions is 0.29 for Hβ(FWHM) and 0.99 for Mg II(FWHM). We conclude that EW or FWHM distributions (for both Hβ and Mg II) are probably independent of the presence or absence of detected microvariability properties in QSOs and Seyferts. As discussed in the Introduction and in more detail in Paper I, if much of the optical emission in RLQSOs comes from a jet, then we would expect the EWs of RLQSOs to be significantly lower than those of RQQSOs and the EWs of microvariable sources to be less than those of non-variable sources. Our results are in agreement with the conclusion in Paper I and thus do not support the hypothesis (e.g. Gopal-Krishna et al. 2003; Czerny et al. 2008) that RQQSOs possess jets that are producing rapid variations. Instead they may

indicate that variations involving the accretion disc (e.g. Wiita 2006) play an important role here.

Further improvements to our results could be obtained through extensive searches for INOV in a larger sample of RQQSOs to reduce the statistical uncertainties. In any such studies, it would be most useful to take the spectra just before or after the photometric monitoring run, so as to ensure the simultaneity of light curves and spectral properties. This would rule out any possibility of change in either of these properties due to temporal gaps between the spectral and photometric epochs; while we very much doubt that this is an important effect, it could have an impact on our results. Such larger samples could be optimally designed if they were made as homogeneous as possible on the basis of apparent magnitudes, redshifts and absolute magnitudes.

REFERENCES

Abazajian K. N. et al., 2009, ApJS, 182, 543
Aihara H. et al., 2011, ApJS, 193, 29
Bochkarev N. G., Gaskell C. M., 2009, Astron. Lett., 35, 287
Boroson T. A., Green R. F., 1992, ApJS, 80, 109
Carini M. T., Noble J. C., Taylor R., Culler R., 2007, AJ, 133, 303
Chand H., Wiita P. J., Gupta A. C., 2010, MNRAS, 402, 1059 (Paper I)
Czerny B., Siemiginowska A., Janiuk A., Gupta A. C., 2008, MNRAS, 386, 1557
Dibai É. A., 1980, SvA, 24, 389
Dietrich M., Mathur S., Grupe D., Komossa S., 2009, ApJ, 696, 1998
Dong X.-B., Wang J.-G., Ho L. C., Wang T.-G., Fan X., Wang H., Zhou H., Yuan W., 2011, ApJ, 736, 86
Dong X.-B., Wang T.-G., Wang J.-G., Fan X., Wang H., Zhou H., Yuan W., 2009b, ApJ, 703, L1
Ferland G. J., Korista K. T., Verner D. A., Ferguson J. W., Kingdon J. B., Verner E. M., 1998, PASP, 110, 761
Fine S. et al., 2008, MNRAS, 390, 1413
Fitzpatrick E. L., 1999, PASP, 111, 63
Gaskell C. M., 2006, in Gaskell C. M., McHardy I. M., Peterson B. M., Sergeev S. G., eds, ASP Conf. Ser. Vol. 360, AGN Variability from X-rays to Radio Waves. Astron. Soc. Pac., San Francisco, p. 111
Gopal-Krishna, Stalin C. S., Sagar R., Wiita P. J., 2003, ApJ, 586, L25
Gupta A. C., Joshi U. C., 2005, A&A, 440, 855
Joshi R., Chand H., Gupta A. C., Wiita P. J., 2011, MNRAS, 412, 2717
Kim D.-C., Sanders D. B., Veilleux S., Mazzarella J. M., Soifer B. T., 1995, ApJS, 98, 129
Mangalam A. V., Wiita P. J., 1993, ApJ, 406, 420
McLure R. J., Dunlop J. S., 2004, MNRAS, 352, 1390
Moustakas J., Kennicutt R. C., Jr, 2006, ApJS, 164, 81
Nilsson K., Pursimo T., Sillanpää A., Takalo L. O., Lindfors E., 2008, A&A, 487, L29
Nilsson K., Pursimo T., Villforth C., Lindfors E., Takalo L. O., 2009, A&A, 505, 601
Rees M. J., 1984, ARA&A, 22, 471
Rokaki E., Collin-Souffrin S., Magnan C., 1993, A&A, 272, 8
Salviander S., Shields G. A., Gebhardt K., Bonning E. W., 2007, ApJ, 662, 131
Schlegel D. J., Finkbeiner D. P., Davis M., 1998, ApJ, 500, 525
Shen Y., Greene J. E., Strauss M. A., Richards G. T., Schneider D. P., 2008, ApJ, 680, 169
Tsuzuki Y., Kawara K., Yoshii Y., Oyabu S., Tanabé T., Matsuoka Y., 2006, ApJ, 650, 57
Vanden Berk D. E. et al., 2001, AJ, 122, 549
Véron-Cetty M.-P., Joly M., Véron P., 2004, A&A, 417, 515
Vestergaard M., Osmer P. S., 2009, ApJ, 699, 800
Vestergaard M., Peterson B. M., 2006, ApJ, 641, 689
Wiita P. J., 2006, in Miller H. R., Marshall K., Webb J. R., Aller M. F., eds, ASP Conf. Ser. Vol. 300, Blazar Variability II: Entering the GLAST Era. Astron. Soc. Pac., San Francisco, p. 183

This paper has been typeset from a TEX/LATEX file prepared by the author.